Peer-reviewed version available at Processes 2018, 6, 184; doi:10.3390/pr6100184

Article

Modeling the separation of microorganisms in bioprocesses by flotation

Stefan Schmideder [1], Christoph Kirse [1], Julia Hofinger [2], Sascha Rollié [2] and Heiko Briesen [1,*]

[1] Technical University of Munich; Chair of Process Systems Engineering; 85354 Freising, Germany
[2] BASF SE; 67056 Ludwigshafen am Rhein, Germany
* Correspondence: heiko.briesen@tum.de; Tel.: +49-8161-71-3272

Abstract: Bioprocesses for the production of renewable energies and materials lack efficient separation processes for the utilized microorganisms such as algae and yeasts. Dissolved air flotation (DAF) and microflotation are promising approaches to overcome this problem. The efficiency of these processes depends on the ability of microorganisms to aggregate with microbubbles in the flotation tank. In this study, different new or adapted aggregation models for microbubbles and microorganisms are compared and investigated for their range of suitability to predict the separation efficiency of microorganisms from fermentation broths. The complexity of the heteroaggregation models range from an algebraic model to a 2D population balance model (PBM) including the formation of clusters containing several bubbles and microorganisms. The effect of bubble and cell size distributions on the flotation efficiency is considered by applying PBMs, as well. To determine the impact of the model assumptions, the modeling approaches are compared and classified for their range of applicability. Evaluating computational fluid dynamics (CFD) of a DAF system shows the heterogeneity of the fluid dynamics in the flotation tank. Since analysis of the streamlines of the tank show negligible backmixing, the proposed aggregation models are coupled to the CFD data by applying a Lagrangian approach.

Keywords: Flotation; Separation of microorganisms; Bioseparation; Heteroaggregation; Population balance modeling; Coupling of aggregation and CFD; Model comparison

1. Introduction

Yeast cells and algae are frequently used in bioprocesses for the production of renewable materials and biofuels [1–4]. The separation of the microorganisms after fermentation is capital and energy intensive. The high separation costs are caused by the small size of microalgae, their growth in very dilute cultures, and their density close to that of water [5,6]. Thus, traditional separation techniques such as filtration, sedimentation, and centrifugation are inefficient [7]. The development of efficient separation processes is essential for the economically feasible production of renewable materials and biofuels.

Dissolved air flotation (DAF) and microflotation are promising approaches to separate microorganisms from the culture broth [6,8–10]. In both flotation principles, microbubbles (bubbles with diameter ranging from 10 to 100 µm) are generated at the inlet to a flotation tank [9,11]. In the flotation tank, the microbubbles and particles aggregate. The particle-bubble aggregates either float into the froth of the tank or are entrained within the clear or recycle stream [12,13]. DAF is already a widely used separation technique in water and wastewater treatment dealing with the removal of cells, algea, and flocs of organic or inorganic materials from water [1,12,14–17]. In order to yield high separation efficiencies, a pre-flocculation process with coagulants can be favorable [1,18,19]. However, to avoid product damage or contamination, flocculation with coagulant should be avoided in some processes [1].

Peer-reviewed version available at Processes 2018, 6, 184; doi:10.3390/pr6100184

Applying suitable modeling approaches can significantly reduce the effort of determining efficient plant configurations and process conditions for flotation. The efficiency of the separation process of microorganisms with DAF or microflotation depends on the ability of microorganisms to aggregate with microbubbles. To our knowledge, there exists no generic and physically correct modeling approach for this heteroaggregation process. Only Zhang et al. (2014) [20] modeled the harvesting of microorganisms with DAF by applying the so called "White Water Blanket Model". They consider the aggregation of several bubbles on single flocs of cells, which are polydisperse in size. However, they neglected the polydispersity of bubbles and the formation of clusters consisting of several bubbles and flocs. In the present study, several mechanistic approaches are taken to model the heteroaggregation between microorganisms and microbubbles in flotation tanks. While still being adapted to the given problem, some of the aggregation models are based on existing models for particle separation by DAF [13,17,21–24]. Other modeling approaches are newly developed in this study. Each model is based on different assumptions for the flotations system: averaged, i.e. homogeneous, loading of cells on bubbles, distributed loading of cells on bubbles, polydispersity of cells, polydispersity of bubbles, and formation of clusters with and without an averaged, i.e. homogeneous, numbers of cells and bubbles. To determine the impact of the presented assumptions, the modeling approaches are compared and classified for their range of applicability. Data of computational fluid dynamics (CFD) of a DAF system show, that the fluid dynamics are highly heterogeneous in the flotation tank and that there is negligible backmixing. Thus, the aggregation models are coupled with the CFD data of the DAF system by using a Lagrangian approach.

2. Modeling approaches

In this study, six different mechanistic models for the heteroaggregation between microbubbles and microorganisms dispersed in a fluid are investigated to calculate the separation efficiency of microorganisms in flotation systems. The aggregation models exhibit different levels of complexity and are applied for two approaches: the classical two zone model [12] with constant flow conditions and the coupling to CFD data by using a Lagrangian approach.

2.1. Aggregation kernel

Each aggregation model contains the aggregation kernel β. The aggregation kernel for the aggregation mechanism i is a combination of the encounter frequency $K_{C,i}$ and the encounter efficiency, which is the probability of an encounter leading to a successful collision [24]:

$$\beta_i = P_{A,i} \cdot P_{C,i} \cdot K_{C,i}, \tag{1}$$

where $P_{A,i}$ and $P_{C,i}$ are the encounter efficiencies due to physiochemical and hydrodynamic effects, respectively. Commonly, the kernels for different mechanisms are superimposed [24,25]:

$$\beta = \beta_L + \beta_S + \beta_T, \tag{2}$$

where β_L, β_S, and β_T are the aggregation kernels due to laminar shear, sedimentation, and turbulent motion. Here, aggregation due to Brownian motion can be neglected, since the cells and bubbles are too large to observe Brownian motion [26]. It is well known [27,28] that an error is made with the linear superimposition, but no closed form including all of the relevant mechanisms exist yet. Furthermore, as the focus of this study is on comparing different models a perfect representation of the kernels is not necessary. Substituting Equation (1) in Equation (2) and assuming that the physiochemical encounter efficiency is independent of the aggregation mechanism, the following relation is obtained

$$\beta = P_A \cdot (P_{C,L} \cdot K_{C,L} + P_{C,S} \cdot K_{C,S} + P_{C,T} \cdot K_{C,T}) . \tag{3}$$

Frequency of encounters

The frequency of encounters is calculated for each mechanism: laminar shear, sedimentation, and turbulent motion. Pedocchi and Piedra-Cueva [29] have extended the frequency of encounters due to laminar shear by von Smoluchowski [30] from a one dimensional formulation to a three-dimensional one (Equation (4) in Table 1), where u, v, and w are the fluid velocities in the x, y, and z directions. To calculate the encounter frequency due to density differences between two different aggregates, Equation (5) in Table 1 has been used [24], where v_1 and v_2 are the rising or settling velocities of the two aggregates 1 and 2. The rising velocity of aggregates consisting of bubbles is set to the rising velocity of single bubbles. For the turbulent encounter frequency, the Saffman-Turner relation is used [27] (Equation (6) in Table 1).

Table 1. Encounter frequencies and efficiencies used for aggregation kernels

	Encounter frequency due to:	
Laminar shear	$K_{S,C} = \frac{1}{6} \cdot (D_1 + D_2)^3 \cdot \sqrt{A}$	(4)
	$A = 2 \cdot \left[\left(\frac{\partial u}{\partial x}\right)^2 + \left(\frac{\partial v}{\partial y}\right)^2 + \left(\frac{\partial w}{\partial z}\right)^2 \right]$	
	$+ \left(\frac{\partial u}{\partial y} + \frac{\partial v}{\partial x}\right)^2 + \left(\frac{\partial u}{\partial z} + \frac{\partial w}{\partial x}\right)^2 + \left(\frac{\partial v}{\partial z} + \frac{\partial w}{\partial y}\right)^2$	
Sedimentation	$K_{G,C} = \frac{\pi}{4} \cdot (D_1 + D_2)^2 \cdot \lvert v_1 - v_2 \rvert$	(5)
Turbulence	$K_{T,C} = \frac{1.3}{8} \cdot (D_1 + D_2)^3 \cdot \sqrt{\frac{\epsilon}{\nu}}$	(6)
	Encounter efficiency due to surface coverage for model:	
Averaged	$P_{A,S}(l) = 1 - l, \quad l \in [0,1]$	(7)
Not Averaged	$P_{A,S}(j) = 1 - \frac{j}{j_{max}}, \quad j \in [0, j_{max}]$	(8)
Poly.Cells	$P_{A,S}(l) = 1 - l, \quad l \in [0,1]$	(9)
Poly.Bubbles	$P_{A,S}(j, d_b) = 1 - \frac{j}{j_{max(d_b)}},$	(10)
	$j \in [1, j_{max(d_b)}]$ and $d_b \in [d_{b_{min}}, d_{b_{max}}]$	
Clustering	$P_{A,S}(i,j,m,l) = R_p(i,j) \cdot R_b(m,l) + R_p(m,l) \cdot R_b(i,j)$	(11)
Clustering Averaged	$P_{A,S}(i,j) = 2 \cdot R_p(i,j) \cdot R_b(i,j),$ for two clusters	(12)
	$P_{A,S}(i,j) = R_b(i,j),$ for a cluster and a cell	(13)
Hydrodynamic encounter efficiency	$P_C = \left(\frac{3}{2} + \frac{4}{15} \cdot \left(\frac{D_2 \cdot U}{\nu}\right)^{0.72} + 37.5 \cdot \Phi\right) \cdot \left(\frac{D_1}{D_2}\right)^2$	(14)

Encounter efficiency

The hydrodynamic encounter efficiency P_C considers the fact that the flow field around the bubble and particle hinders aggregation [31,32]. P_C can be expressed as Equation (14) in Table 1, where D_1 and D_2 are the diameter of the particle and bubble, ν is the kinematic viscosity of the fluid, and Φ is the gas volume fraction. This efficiency was derived for dirty interfaces [31,32], which is valid here, because the flotation bubbles are created in a complex medium that will dirty the interface shortly after bubble creation. This correlation used for P_C neglects, e.g. effects of density differences [33], but again the focus is not a perfect representation of the kernels but a model comparison. The characteristic velocity U depends on the aggregation mechanism. According to Kostoglou et al. [25] and Dai et al. [34] the characteristic velocities for laminar shear and sedimentation are the rising velocities of the bubbles. The average relative velocity U_T due to turbulent motion can be expressed as [25]

$$U_T = \frac{5}{2\Pi} \cdot \sqrt{\frac{\epsilon}{15\nu}} \cdot (D_1 + D_2), \tag{15}$$

where ϵ is the turbulent dissipation.

The encounter efficiency $P_A = P_{A,S} \cdot P_{A,0}$ allows describing space limitations on the bubble $P_{A,S}$ [13,23] or other effects such as repulsion and attractive forces $P_{A,0}$ [35]. Repulsion and attractive forces depend heavily on the process conditions and can be influenced by the addition of chemicals that tailor surface properties of cells or bubbles. They can either be modeled using the DLVO theory extended

by Born repulsion forces [36] or be computed using molecular dynamics simulations [37], which requires knowledge of the surface of the particles, or be measured using atomic force microscopy [38]. Using those methods to infer $P_{A,0}$, the effect of chemical addition on separation efficiency should become predictable with a suitable aggregation model. Nevertheless, most of the studies on DAF estimate $P_{A,0}$ from empirical relations or by fitting experimental data [17,23]. Since this study describes the generalized modeling of flotation processes, $P_{A,0}$ is set to one. Most studies on DAF processes, including this one, consider that surface coverage reduces the encounter efficiency and assume that the encounter efficiency is proportional to the ratio of the remaining free surface to the total surface. The cells occupy their projected surface area on the bubble surface [13,17,23]. The development of layers with multiple cells on the surface of bubbles is neglected in this study, since it is assumed that the cells do weakly aggregate with others. If the cells would aggregate, one could easily use a coagulation unit prior to flotation to increase the size of the cell-aggregates and the flotation efficiency.

2.2. Spatial models

There exist two different approaches to model the separation efficiency in DAF tanks. The traditional approach divides the DAF tank into the contact zone and the separation zone [11–13,23]. More advanced approaches combine CFD simulations with the aggregation process in flotation tanks [24,25,39]. In this study both approaches are examined and applied to the different aggregation models.

Two zone model

It is assumed that aggregation only occurs in the contact zone, where bubbles and cells enter the inlet and aggregate until the outlet of the contact zone. Since plug flow with constant flow conditions is assumed, the introduced substantial derivatives for the aggregation models in Section 2.3 simplify to time derivatives. The terms for the change of the bubble concentration over time due to velocity differences between bubbles and the fluid can be neglected. Furthermore, no aggregation occurs in the flotation zone and all cells, which have been attached onto bubbles in the contact zone float and are thus removed. The separation efficiency η is calculated as

$$\eta = 1 - \frac{c_{c_{outlet}}}{c_{c_{inlet}}}, \tag{16}$$

where $c_{c_{outlet}}$ and $c_{c_{inlet}}$ are the concentrations of unbounded cells at the outlet and at the inlet of the contact zone, respectively.

Lagrangian model

To combine CFD simulations with the aggregation process in DAF tanks, an Euler/Euler CFD simulation (for the commercially available DAF system Enviplan: AQUATECTOR®Microfloat®, see Figure 5a for a two phase system consisting of the liquid and gaseous phase has been performed with Ansys Fluent. The gaseous phase was described by bubbles with a diameter of 40 µm and a density of an air bubble with a maximum loading of microorganisms (18.28 kg/m^3). Those estimates were based on experimental data for the flotation of yeasts (data not shown). For the liquid phase, water properties were applied. The central inlet was a mass flow inlet, the free surface a degassing boundary and one bottom opening (side) a pressure outlet. The mesh consisted of hexahedral cells (approximately 0,5 Mio. elements). Most of the tank was expected to be laminar, while the inlet region had a Reynolds number in the turbulent regime. Therefore, different turbulence models (k-omega SST, k-epsilon) and a model without turbulence (laminar) were evaluated but no effect on gas hold-up or flow field was observed. For drag on the bubbles, the model by Tomiyama et al. [40] was used.

In order to combine CFD results and aggregation processes, several streamlines are tracked. While unbounded cells are assumed to follow the fluid streamline until the outlet is reached, the concentration of bubbles decreases on the course of a streamline due to velocity differences between bubbles and the fluid. This is included in the formulation of the aggregation models in Section 2.3 by substantial

derivatives and the included terms for the time dependent change of the bubble concentration. The change of the bubble concentration is combined with the CFD simulations. CFD results also show that unloaded bubbles and loaded bubbles behave very similar. Thus, it is assumed that free bubbles and bubble-particle aggregates behave in the same way.

Additionally, CFD data show, that the gas volume fraction in the outlet of the flotation tank is negligible (see Figure 5). Assuming that bubble-cell aggregates behave like unloaded bubbles, all cells, which are attached to bubbles, float. Only the unbounded cells remaining in the outlet do not float. Thus, the separation efficiency for the Lagrangian model is calculated as described in Equation (16). The recycling of the outlet is generally implementable in the introduced models but not included in the given study. The integration of heteroaggregation processes and CFD data by the realized Lagrangian approach poses a sufficient and useful method for design evaluation. Full coupling can be done in a future step and might be interesting if bubble dynamics might be affected by significant change in bubble density and corresponding effects on fluid dynamics.

2.3. Heteroaggregation modeling

In this section the applied models for the heteroaggregation between microbubbles and cells (Figure 1) are described.

Peer-reviewed version available at Processes 2018, 6, 184; doi:10.3390/pr6100184

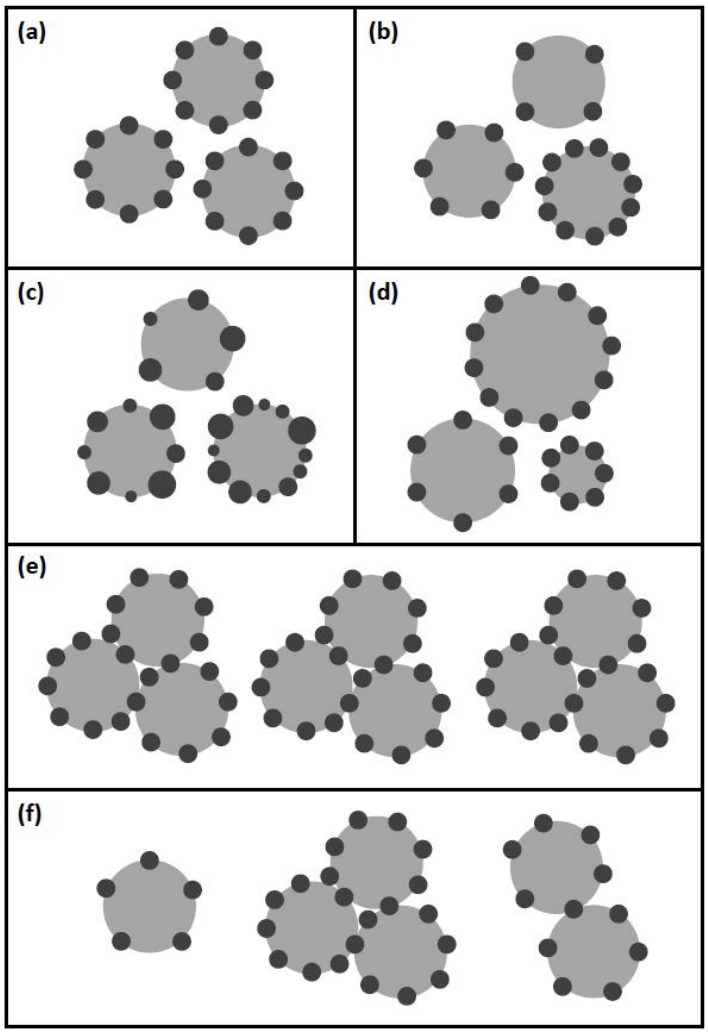

Figure 1. Illustration of the different aggregation models, where grey spheres represent bubbles and dark spheres correspond to microorganisms: (a) *Averaged*: several monodisperse cells aggregate on monodisperse bubbles; loading of bubbles is averaged; (b) *Not Averaged*: several monodisperse cells aggregate on monodisperse bubbles; loading of bubbles is distributed; (c) *Poly.Cells*: several polydisperse cells aggregate on monodisperse bubbles; (d) *Poly.Bubbles*: several monodisperse cells aggregate on polydisperse bubbles; (e) *Clustering Averaged*: formation of aggregates with multiple monodisperse bubbles and monodisperse cells; bubble and cell number per cluster is averaged; (f) *Clustering*: formation of aggregates with multiple monodisperse bubbles and monodisperse cells; bubble and cell number per cluster is distributed

Averaged

The model *Averaged* describes the aggregation of multiple cells on larger bubbles. Moreover, the bubbles and cells are assumed to be monodisperse in their size and shape. The loading of bubbles with cells is assumed to be uniform, i.e. each bubble's surface area is occupied with cells in the same manner. The general equation for aggregation between cells and bubbles is

$$\frac{\mathrm{D}c_c}{\mathrm{D}t} = -\beta(d_c, d_b, \boldsymbol{X}) \cdot c_c \cdot c_b \tag{17}$$

where c_c and c_b are the number concentrations of unbounded cells, respectively bubbles, t is the time, and d_c and d_b are the diameter of the cells and bubbles, respectively. If the conditions are not homogeneous throughout the tank, that causes a dependence of the aggregation kernel on the position

$\boldsymbol{X}$. The encounter efficiency due to surface coverage is calculated by Equation (7) in Table 1, where l is the ratio of the occupied and total surface area of a bubble. Applying the Lagrangian approach, the velocity difference between bubbles and the fluid causes a change of the bubble concentration on the course of a streamline

$$\frac{\mathrm{D}c_b}{\mathrm{D}t} = \frac{c_b}{\Phi} \cdot \frac{\mathrm{d}\Phi}{\mathrm{d}t}, \tag{18}$$

where the gas volume fraction Φ and its time dependent change was obtained from CFD data in this study.

Not Averaged

In contrast to the model *Averaged*, the loading of bubbles with cells is not assumed to be uniform in the model *Not Averaged*, i.e. there exists a number density distribution of bubbles loaded with a different amount of cells. Therefore, models where multiple bubbles can aggregate on larger particles [17,21,22] have been adapted to a population balance model for the aggregation of several cells on larger bubbles. Thus, a bubble with j attached cells can be formed by the aggregation between a bubble with $j-1$ attached cells and a single cell. If a bubble with j attached cells aggregates with one more cell, a bubble with $j+1$ cells is created. The model results in a 1D discrete population balance model, in which bubbles are loaded with a discrete number of cells.

$$\begin{aligned}
\frac{\mathrm{D}c_0}{\mathrm{D}t} &= -\beta(d_c, d_b, j=0, \boldsymbol{X}) \cdot c_c \cdot c_0 + \frac{c_0}{\Phi} \cdot \frac{\mathrm{d}\Phi}{\mathrm{d}t} \\
\frac{\mathrm{D}c_j}{\mathrm{D}t} &= \beta(d_c, d_b, j-1, \boldsymbol{X}) \cdot c_c \cdot c_{j-1} - \beta(d_c, d_b, j, \boldsymbol{X}) \cdot c_c \cdot c_j \\
&\quad + \frac{c_j}{\Phi} \cdot \frac{\mathrm{d}\Phi}{\mathrm{d}t}, \qquad j \in [1, j_{max}-1] \\
\frac{\mathrm{D}c_{j_{max}}}{\mathrm{D}t} &= \beta(d_c, d_b, j_{max}-1, \boldsymbol{X}) \cdot c_c \cdot c_{j_{max}-1} + \frac{c_{j_{max}}}{\Phi} \cdot \frac{\mathrm{d}\Phi}{\mathrm{d}t}
\end{aligned} \tag{19}$$

$$\frac{\mathrm{D}c_c}{\mathrm{D}t} = \sum_{j=0}^{j_{max}-1} -\beta(d_c, d_b, j, \boldsymbol{X}) \cdot c_c \cdot c_j, \tag{20}$$

where c_c is the number concentration of unbounded cells and c_j is the number density of monodisperse bubbles loaded with j cells. The physiochemical collision efficiency $P_A(j)$, for a bubble already having j attached cells (compare with [23]) can be expressed as Equation (8) in Table 1, where $j_{max} = \frac{4 \cdot d_b^2}{d_c^2}$ is the maximum number of cells that can attach to a bubble.

Poly.Cells

In the model *Poly.Cells*, the bubbles are still assumed to be monodisperse, whereas cells are polydisperse in size. Since cells are polydisperse, the surface coverage of bubbles is continuous. Thus, bubbles have the occupancy level l, which is the ratio between the occupied and total surface area of a bubble. Each cell diameter is assigned a specific occupancy potential p, which can be expressed as

$$p(d_c) = \frac{A_{c,projected}}{A_{b,surface}} = \frac{d_c^2}{4 \cdot d_b^2}, \tag{21}$$

where $A_{c,projected}$ is the projected surface area of a cell and $A_{b,surface}$ is the surface area of a bubble. Due to a aggregation with a cell with the occupancy potential p, the occupancy level of a bubble increases from l_0 to $l = l_0 + p$. The set of equations for the 1D continuous population balance model is

$$\begin{aligned}\frac{\mathrm{D}c_b(l)}{\mathrm{D}t} =& \int_{p=p_{min}}^{p_{max}} \beta(d_c, d_b, l-p, p, \boldsymbol{X}) \cdot c_b(l-p) \cdot c_c(p)\,\mathrm{d}p \\ & - c_b(l) \cdot \int_{p=p_{min}}^{l_{max}-l} \beta(d_c, d_b, l, p, \boldsymbol{X}) \cdot c_c(p)\,\mathrm{d}p \\ & + \frac{c_b(l)}{\Phi} \cdot \frac{\mathrm{d}\Phi}{\mathrm{d}t}, \qquad\qquad l \in [0,1] \end{aligned} \tag{22}$$

$$c_b(l) = 0 \quad \text{for } l < 0 \tag{23}$$

$$\frac{\mathrm{D}c_c(p)}{\mathrm{D}t} = -c_c(p) \cdot \int_{l=l_{min}}^{l_{max}-p} \beta(d_c, d_b, l, p, \boldsymbol{X}) \cdot c_b(l)\,\mathrm{d}l, \qquad p \in [p_{min}, p_{max}], \tag{24}$$

where $c_c(p)$ is the number density of polydisperse cells with the occupancy potential p and $c_b(l)$ is the number density of monodisperse bubbles with the occupancy level l. $P_{A,Surface}$ is described in Equation (9) in Table 1.

Poly.Bubbles

The models by Fukushi et al. [13] and Matsui et al. [23] have been adapted to the heteroaggregation between smaller monodisperse cells on larger polydisperse bubbles. That results in a population balance, in which the discrete property is the loading of cells on bubbles and the continuous property is the size of bubbles

$$\left.\begin{aligned}\frac{\mathrm{D}c_0(d_b)}{\mathrm{D}t} =& -\beta(d_c, d_b, j=0, \boldsymbol{X}) \cdot c_c \cdot c_0(d_b) + \frac{c_0(d_b)}{\Phi} \cdot \frac{\mathrm{d}\Phi}{\mathrm{d}t} \\ \frac{\mathrm{D}c_j(d_b)}{\mathrm{D}t} =& \beta(d_c, d_b, j-1, \boldsymbol{X}) \cdot c_c \cdot c_{j-1}(d_b) \\ & - \beta(d_c, d_b, j, \boldsymbol{X}) \cdot c_c \cdot c_j(d_b) + \frac{c_j(d_b)}{\Phi} \cdot \frac{\mathrm{d}\Phi}{\mathrm{d}t} \\ \frac{\mathrm{D}c_{j_{max}}(d_b)}{\mathrm{D}t} =& \beta(d_c, d_b, j_{max}-1, \boldsymbol{X}) \cdot c_c \cdot c_{j_{max}-1}(d_b) \\ & + \frac{c_{j_{max}}(d_b)}{\Phi} \cdot \frac{\mathrm{d}\Phi}{\mathrm{d}t} \end{aligned}\right\} \begin{aligned} d_b \in & [d_{b_{\min}}, d_{b_{\max}}] \\ j \in & [1, j_{\max}-1] \end{aligned} \tag{25}$$

$$\frac{\mathrm{D}c_c}{\mathrm{D}t} = \int_{d_b=d_{b_{min}}}^{d_{b_{max}}} \sum_{j=0}^{j_{max}-1} -\beta(d_c, d_b, j, \boldsymbol{X}) \cdot c_c \cdot c_j(d_b)\,\mathrm{d}_b, \tag{26}$$

where $c_j(d_b)$ is the number density of bubbles with the diameter d_b and j attached cells. The number concentration of unbounded cells is represented as c_c. The maximum number of cells that can attach to a single bubble $j_{max}(d_b) = \frac{4 \cdot d_b^2}{d_c^2}$ depends on the respective bubble diameter. The minimum and maximum bubble diameter are defined as $d_{b_{min}}$ and $d_{b_{max}}$. The encounter efficiency due to surface coverage is calculated as in Equation (10) in Table 1.

Clustering

The model *Clustering* is based on the model by Lakghomi et al. [24], in which clusters of bubbles and particles were considered. In this study clustering is the formation of aggregates with multiple bubbles and cells, where both, bubbles and cells are assumed to be monodisperse. This results in a discrete bivariate population balance model

$$\frac{\mathrm{DC}_{i,j}}{\mathrm{D}t} = \frac{1}{2} \cdot \sum_{m=0}^{i} \sum_{l=0}^{j} \beta(d_c, d_b, i, j, m, l, \boldsymbol{X}) \cdot C_{m,l} \cdot C_{i-m,j-l} - \sum_{m=0}^{i_{max}-i} \sum_{l=0}^{j_{max}-l} \beta(d_c, d_b, i, j, m, l, \boldsymbol{X}) \cdot C_{i,j} \cdot C_{m,l} + \frac{C_{i,j}}{\Phi} \cdot \frac{\mathrm{d}\Phi}{\mathrm{d}t}, \qquad \text{for } i > 0 \tag{27}$$

$$\frac{\mathrm{DC}_{0,1}}{\mathrm{D}t} = - \sum_{m=0}^{i_{max}} \sum_{l=0}^{j_{max}-l} \beta(d_c, d_b, i, j, m, l, \boldsymbol{X}) \cdot C_{0,1} \cdot C_{m,l}, \tag{28}$$

where $C_{i,j}$ is the number density of clusters with i bubbles and j cells. Contrary to Lakghomi et al. [24], in this study, the reduction of the encounter efficiency due to surface coverage is included. It is assumed that aggregation between two clusters can only occur, if a cell on the exposed surface of a cluster collides with a bubble on the exposed surface of the other cluster or vice versa. Then $P_{A,surface}$ between a cluster with i bubbles and j cells (Cluster 1) and a cluster with m bubbles and l cells (Cluster 2) can be expressed as described in Equation (11) in Table 1. $R_p(i,j)$ and $R_b(i,j)$ are the fractions of the exposed cluster surface area of Cluster 1 which is occupied by cells and bubbles, respectively. The derivations for R_p and R_b are described in the Appendix B.

There is no suitable approach to model the hydrodynamic encounter efficiency between two clusters consisting of bubbles and particles in literature. Thus, the hydrodynamic encounter efficiency P_C for the case of clustering has been simplified. The expression by Kostoglou et al. [25] is used for the hydrodynamic encounter efficiency of single cells and clusters consisting of one or more bubbles. For two clusters, both containing one ore more bubbles, the hydrodynamic encounter efficiency is predicted to be close to 1 by this model. Therefore, a value of 1 is used for P_C.

Clustering Averaged

For the model *Clustering Averaged* it is assumed that all clusters have the same number of bubbles and cells. The number concentration of free cells c_c decreases over time due to aggregation with clusters, whereas the number concentration of clusters c_{Agg} decreases due to the aggregation of two clusters and due to the velocity difference between bubbles and the fluid. The average number of bubbles and cells per cluster i and j can be described as well. The product of c_{Agg} and i does only change due to the velocity difference between bubbles and the fluid, whereas the product of c_{Agg} and j additionally increases due to the aggregation of unbounded cells. The initial number concentration of clusters is equal to the initial bubble number concentration.

$$\frac{\mathrm{D}c_c}{\mathrm{D}t} = - \beta(i, j, d_c, d_b, \boldsymbol{X}) \cdot c_c \cdot c_{Agg} \tag{29}$$

$$\frac{\mathrm{D}c_{Agg}}{\mathrm{D}t} = - \beta(i, j, d_c, d_b, \boldsymbol{X}) \cdot c_{Agg}^2 + \frac{c_{Agg}}{\Phi} \cdot \frac{\mathrm{d}\Phi}{\mathrm{d}t} \tag{30}$$

$$\frac{\mathrm{D}\left(c_{Agg} \cdot i\right)}{\mathrm{D}t} = \frac{c_{Agg} \cdot i}{\Phi} \cdot \frac{\mathrm{d}\Phi}{\mathrm{d}t} \tag{31}$$

$$\frac{\mathrm{D}\left(c_{Agg} \cdot j\right)}{\mathrm{D}t} = \beta(i, j, d_c, d_b, \boldsymbol{X}) \cdot c_c \cdot c_{Agg} + \frac{c_{Agg} \cdot j}{\Phi} \cdot \frac{\mathrm{d}\Phi}{\mathrm{d}t} \tag{32}$$

The encounter efficiency due to surface coverage between two identical cluster or between a cluster and an unbounded cell can be calculated with Equation (12) and (13) in Table 1. Equivalent to the model *Clustering*, Equation (14) is used for the hydrodynamic encounter efficiency of single cells and clusters consisting one ore more bubbles. For two identical clusters, the hydrodynamic collision efficiency is close to one and therefore set to one.

3. Numerical methods

In this study, all ODEs are solved with the MATLAB solver ode45. The models *Averaged*, *Not Averaged* and *Clustering Averaged* consist of a set of ordinary differential equations (ODEs). For the model *Poly.Bubbles*, the bubbles are classified into discrete bubble sizes. The bubbles are loaded with a discrete number of cells which results in a discrete set of ODEs. To solve the model *Poly.Cells*, the cells are classified into a discrete number of cells. The loading of the bubbles is classified into discrete occupancy levels. Due to the aggregation of a bubble with a cell, the new occupancy level of the bubble is in between two discrete classes for the occupancy level. Therefore, the new built aggregates have to be divided onto neighboring nodes. For this purpose, the cell average technique is used [41] to obtain a discrete set of ODEs. In order to test for grid convergence, simulations were also performed with a finer resolution and no difference in the results was observed. To obtain a discrete number of ODEs for the model *Clustering*, the maximum numbers of bubbles and cells for a cluster are limited to a discrete number. If the aggregation between two clusters would form a cluster, which would be outside of this limiting region, the aggregation process is set to be impossible. The maximum numbers of bubbles and cells for a cluster are chosen sufficiently high, i.e. the formation of clusters beyond the limiting region is rare (data not shown). Applying lower tolerances for the ODE solver than used in this study did not change the results.

4. Results and discussion

First, the impact of the assumptions of the different aggregation models and the effects leading to the formation of clusters are investigated assuming a two zone model. Then, the focus is set on the spatial aggregation in a commercially available DAF system (Enviplan: AQUATECTOR®Microfloat® Rundzelle). To compare different simulations, a set of standard parameters (Table 2) is introduced. The parameters have been used for the simulations, unless other parameter settings are mentioned. The turbulence dissipation rate and the shear rate are chosen in a range as observed at the inlet of the investigated flotation tank. The residence time is chosen arbitrarily, whereas the other standard parameters are set to reasonable values.

Table 2. Standard parameters for simulations

Parameter	Abbreviation	Value	Unit
Residence time	$t_{residence}$	10	s
Gas volume fraction	Φ	0.03	-
Bubble diameter	d_b	40	μm
Cell diameter	d_c	5	μm
Cell concentration of feed	c_{feed}	10	$g\,L^{-1}$
Ratio recycle flow to total flow	$\frac{\dot{V}_{Recycle}}{\dot{V}_{Total}}$	$\frac{5}{6}$	-
Viscosity fluid	μ	0.89	$mPa\,s$
Turbulent dissipation rate	ϵ	0.0025	$m^2\,s^{-3}$
Shear rate	$\dot{\gamma}$	$\sqrt{125}$	s^{-1}

4.1. Comparison of the different aggregation models

In this section the heteroaggregation models are compared, whereby a plug flow is assumed, i.e. flow conditions stay constant during the simulation. For constant flow conditions, the model *Averaged* has an analytical solution which is derived in the Appendix A. The analytical solution includes the dimensionless groups Π_1 and Π_3

$$\Pi_1 = \frac{1}{4} \cdot \frac{c_{c,0} \cdot d_{c,0}^2}{c_{b,0} \cdot d_{b,0}^2} \tag{33}$$

$$\Pi_3 = t_{residence} \cdot \beta_{unloaded}(d_{c,0}, d_{b,0}) \cdot c_{b,0}, \tag{34}$$

Preprints (www.preprints.org) | NOT PEER-REVIEWED | Posted: 22 August 2018 doi:10.20944/preprints201808.0396.v1

Peer-reviewed version available at Processes 2018, 6, 184; doi:10.3390/pr6100184

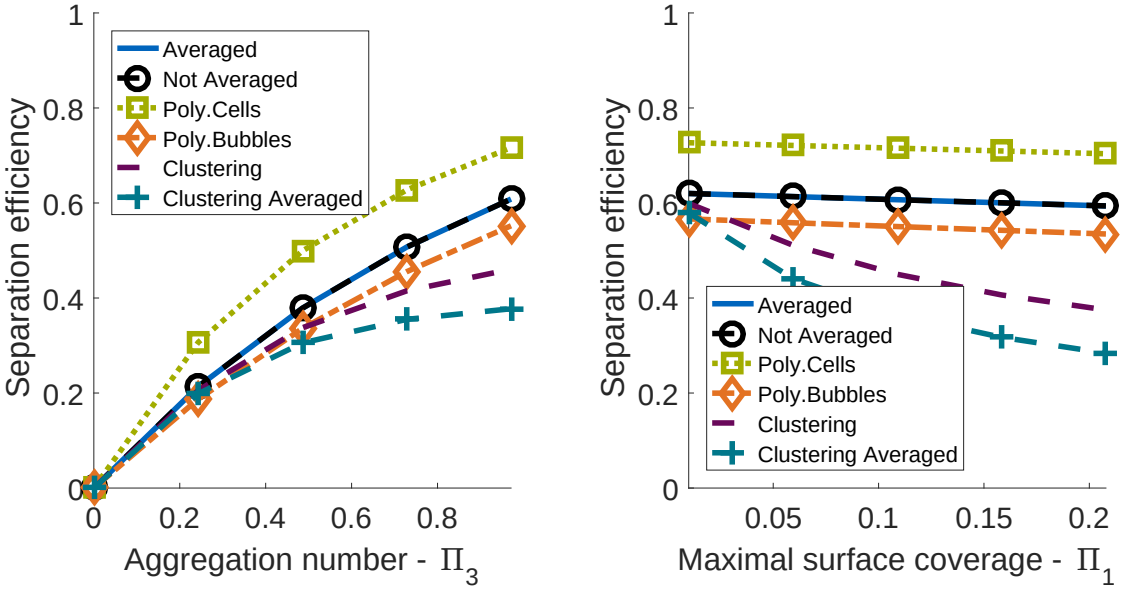

(a) Separation efficiency depending on aggregation number at $\Pi_1 = 0.099$

(b) Separation efficiency depending on maximal surface coverage at $\Pi_3 = 0.971$

Figure 2. Comparison between the different aggregation models (*Poly.Cells*: $\sigma_{rel}(d_c) = 0.25$; *Poly.Bubbles*: $\sigma_{rel}(d_b) = 0.25$)

where $c_{c,0}$ is the initial number concentration of cells, $c_{b,0}$ the initial bubble concentration, $t_{residence}$ the residence time in the contact zone, and $\beta_{unloaded}(d_{c,0}, d_{b,0})$ the aggregation kernel for cells and unloaded bubbles. Π_1 is the fraction of the initial bubble surface area that can be theoretically occupied by the cells assuming the most favorable aggregation conditions. A high aggregation number Π_3 corresponds to frequent aggregation. For the standard parameter settings $\Pi_1 = 0.099$ and $\Pi_3 = 0.971$.

The separation efficiencies of the heteroaggregation models are calculated with Equation (16) and plotted over the two dimensionless groups Π_1 and Π_3 (Figure 2). If $\Pi_3 = 0$, the efficiency is zero, because no aggregation can occur. Then, the efficiency increases with an increasing aggregation number, since a high aggregation number results from favorable collision conditions. A high Π_1 results from a high ratio between the projected surface of all cells and the surface of all bubbles. Thus, the efficiency decreases with an increasing Π_1. To calculate the separation efficiency as described in Equation (16), Π_1 has to be chosen $\Pi_1 > 0$. For very small values of Π_1, the separation efficiencies of the different models show already differences.

No difference between the models *Averaged* and *Not Averaged* can be observed in the entire range of the dimensionless groups Π_1 and Π_3. It can be observed, that the loading of the bubbles for the model *Averaged* approximately equals to the mean loading of bubbles for the model *Not Averaged* (data not shown).

The cell size distribution of microorganisms can be described by a gamma distribution [42], which allows setting the mean value and the standard deviation and guarantees positive diameters. Thus, in the model *Poly.Cells* the initial cell size distribution is set to a gamma distribution. In our model, the mean diameter is equal to the standard parameter $d_{c,mean} = 5\,\mu m$ and the relative standard deviation $\sigma_{rel} = \frac{\sigma}{d_{c,mean}}$ is 0.25. The efficiency of the model *Poly.Cells* is higher than the efficiency of the model *Averaged* in the entire range of Π_3 and Π_1, which is discussed in detail in the next section. Additionally, the difference between the two models tends to increase with higher relative standard deviations of the cell diameter (data not shown). For the model *Poly.Cells*, the initial bubble size distribution

is assumed to be a gamma distribution with the mean diameter equal to the standard parameter $d_{b,mean} = 40\,\mu m$ and $\sigma_{rel} = 0.25$. The efficiency of the model with polydisperse bubbles is lower than the efficiency of the model *Averaged* for the entire ranges of the dimensionless groups Π_1 and Π_3. A possible explanation for this observation is, that most of the bubbles' volume is represented in larger bubble sizes, since the volume of a single bubble is proportional to the bubble diameter cubed. However, large bubbles are less efficient in floating cells than small bubbles [12]. The ratio between the surface and the volume of a bubble decreases with an increasing bubble diameter. This results in an increased maximal surface coverage and a decreased flotation efficiency for larger bubbles.

The lower the standard deviations of the models *Poly.Cells* and *Poly.Bubbles*, the more similar are the results compared to the model *Averaged* (data not shown).

The separation efficiencies of the models *Clustering* and *Clustering Averaged* are lower than the separation efficiencies of the model *Averaged* in the whole range of Π_1 and Π_3. Additionally, the model *Clustering Averaged* yields lower separation efficiencies than the model *Clustering*. This could be caused by an overestimation of the cluster formation for the model *Clustering Averaged*. In general, clustering reduces the efficiency because the formation of clusters with multiple bubbles reduces the available surface area of bubbles. Therefore, the frequency of the attachment of cells decreases.

4.1.1. Influence of the cell size distribution

To investigate the influence of a distributed cell diameter on the efficiency of the flotation process, the number density distribution of unbounded cells is computed at different simulation times (see Figure 3) for the model *Poly.Cells*. The applied relative standard deviation is $\sigma_{rel} = 0.25$. Each distribution below the initial distribution signifies a subsequent simulation time. Due to aggregation with bubbles the number density distribution of free cells decreases with an increasing simulation time. Furthermore, the number density of bigger cells decreases significantly faster than the number densities of smaller cells. Since the mass of a single cell is proportional to the cell diameter cubed, most of the mass of the cells is represented in larger cell sizes and aggregates quite fast. Therefore, the efficiency increases using a gamma distribution for the cell diameter as can be observed in Figure 2.

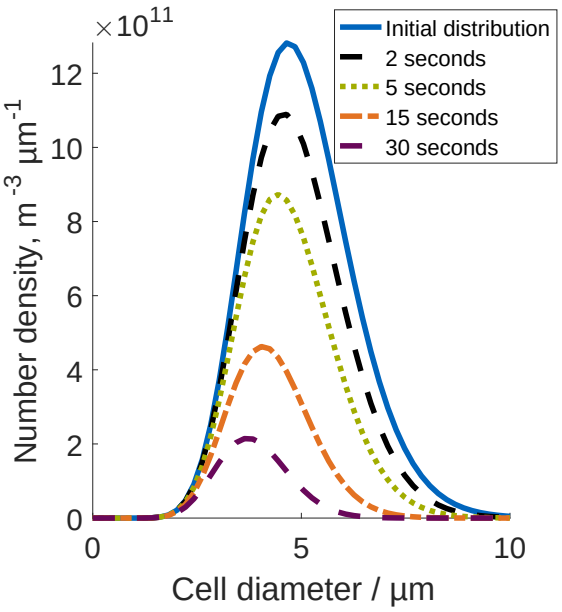

Figure 3. Number density distribution of unbounded cells for the model *Poly.Cells* at different simulation times; standard parameter are used and $\sigma_{rel} = 0.25$

Preprints (www.preprints.org) | NOT PEER-REVIEWED | Posted: 22 August 2018 doi:10.20944/preprints201808.0396.v1

Peer-reviewed version available at Processes 2018, 6, 184; doi:10.3390/pr6100184

4.1.2. Mechanisms leading to the formation of clusters

To detect the main effects influencing the formation of aggregates with multiple bubbles, the influence of the flow conditions are investigated. The turbulent dissipation rate ϵ and the shear rate $\dot{\gamma}$ are varied, while the dimensionless groups Π_1 and Π_3 are kept constant (see Figure 4a). Thus, the aggregation mechanisms due to laminar shear and turbulent motion are varied. The turbulent dissipation rate ϵ and the shear rate $\dot{\gamma}$ are plotted depending on their standard parameters ϵ_{St} and $\dot{\gamma}_{St}$. Since Π_1 and Π_3 are kept constant, the efficiency for the analytical model does not change over the entire parameter range. In absence of shear and turbulence $\epsilon = \dot{\gamma} = 0$, the separation efficiencies of the models *Clustering* and *Averaged* are equal. With increasing ϵ and $\dot{\gamma}$, the efficiency of the clustering model decreases significantly. Figure 4b illustrates two number density distributions of clusters with a certain bubble number at a residence time of 10 seconds. Therein, the green dots represent the simulation of the model *Clustering* with no turbulence and no shear, i.e., $\epsilon/\epsilon_{St} = 0$ and $\dot{\gamma}/\dot{\gamma}_{St} = 0$. The orange dots represent the simulation with the standard parameters for $\epsilon = \epsilon_{St}$ and $\dot{\gamma} = \dot{\gamma}_{St}$. In the case of no turbulence and no shear, it can be observed, that there are almost no aggregates consisting of more than one bubble. The aggregation mechanism is only due to sedimentation. This aggregation mechanism does not seem to cause clustering of aggregates with multiple bubbles significantly. On the contrary, for high turbulence and high shear, aggregates consisting of several bubbles are formed. This lowers the efficiency, since the available surface of bubbles decreases, where cells can aggregate. It can be deduced, that shear and turbulence cause clustering.

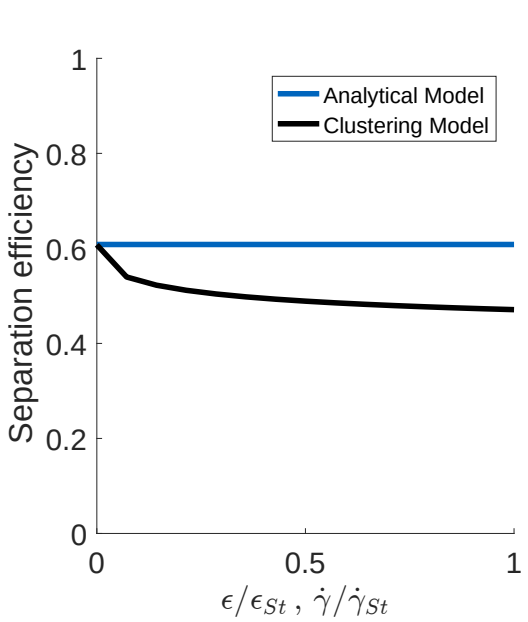

(a) Separation efficiency.

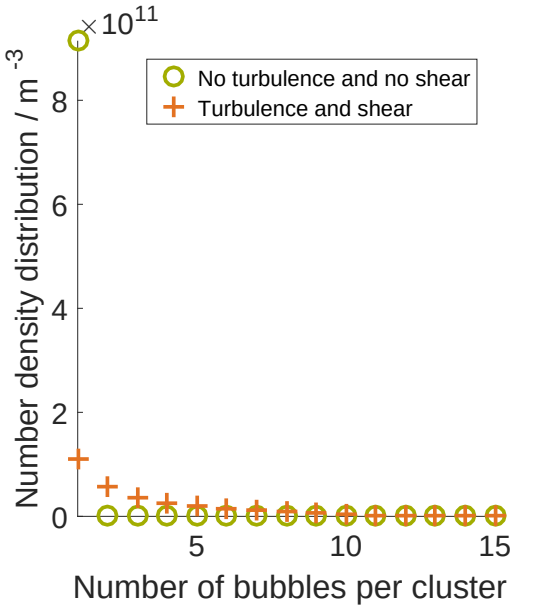

(b) Number density distribution of clusters for the two extreme cases.

Figure 4. Investigation on effect of variation of turbulent eddy dissipation and shear rate for constant Π_1 and Π_3 on cluster formation.

4.1.3. Scope of aggregation models

The properties and scopes for the different aggregation models are illustrated in Table 3. Due to comparable modeling approaches, the separation efficiencies for the aggregation models are identical for the case of monodisperse cells and bubbles and without turbulence and laminar shear (data not shown). Considering effects like clustering or a cell and bubble size distribution increases the power

Preprints (www.preprints.org) | NOT PEER-REVIEWED | Posted: 22 August 2018 doi:10.20944/preprints201808.0396.v1

Peer-reviewed version available at Processes 2018, 6, 184; doi:10.3390/pr6100184

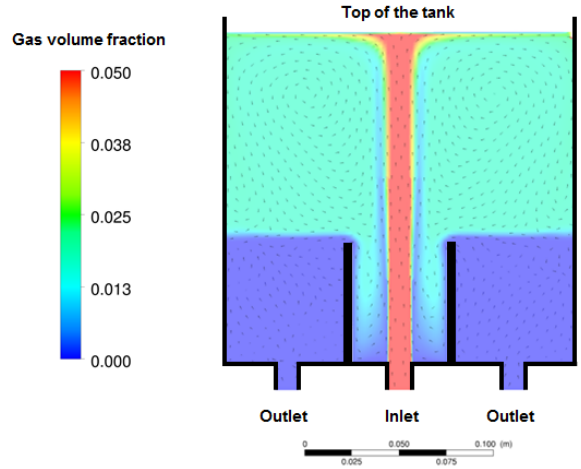

(a) Gas volume fraction and velocity directions of fluid

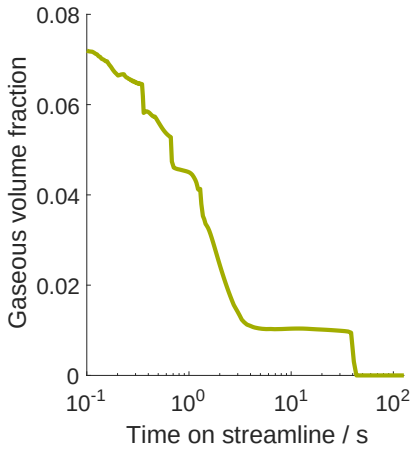

(b) Evolution of the gas volume fraction of a single streamline

Figure 5. Process conditions of the investigated flotation tank

of the aggregation model but also the simulation time. If cell and bubble sizes show small standard deviations, the models *Averaged*, *Not Averaged*, *Clustering* and *Clustering Averaged* can be used for model based optimization. Generally, the model *Averaged* should be preferred to the model *Not Averaged* for determining efficient plant configurations and process conditions, since it requires much less computational and modeling efforts and yields the same results. Since polydispersity of cells and bubbles influence the efficiency, cell and bubble diameter distributions should be considered for quite high standard deviations by using the models *Poly.Cells* or *Poly.Bubbles*. Turbulence and laminar shear cause the formation of clusters, which lowers the flotation efficiency. Due to the low simulation time and complexity, the model *Clustering Averaged* may be preferred to the model *Clustering* for direct coupling to CFD, if turbulence and laminar shear are sufficiently high to require consideration of cluste formation. The two clustering models are also applicable, if the cells exist as aggregates which are bigger than the microbubbles.

4.2. Lagrangian approach

In this section, the aggregation models are coupled with Euler/Euler CFD simulations for the commercially available DAF system from Enviplan (AQUATECTOR®Microfloat®) with a flow rate of 75 l/h. The geometry and the distribution of the gas volume fraction of the tank are illustrated in Figure 5a. From the inlet to the top of the tank, the gas volume fraction is quite high in a narrow area, which is the main stream of the tank. At the top of the tank, most of the bubbles remain in the foam. The other areas of the tank do not have such a high gas volume fraction. Close to the outlet, Φ is zero. Exemplarily, the heteroaggregation on one streamline of the DAF tank is investigated in detail.

4.2.1. Gas volume fraction

The investigated streamline has a residence time of about 140 seconds. The development of the gas volume fraction is illustrated in Figure 5b. Examining the coordinates of the CFD data (not illustrated here) shows, that the top of the tank is reached in about 1.5 seconds. After approximately 3 seconds the streamline leaves the top of the tank and flows to the outlet. During this time, Φ drops from 0.07 to 0.01. At the lower part of the tank, Φ is zero. With the assumption that bubble-cell aggregates behave like unloaded bubbles, all cells, which are attached to bubbles, float. Only the unbound cells remaining in the outlet do not float and get washed out of the tank.

Peer-reviewed version available at Processes 2018, 6, 184; doi:10.3390/pr6100184

Table 3. Properties and scopes of aggregation models

	Averaged	*Not Averaged*	*Poly.Cells*	*Poly.Bubbles*	*Clustering*	*Clustering Averaged*
Cells polydisperse	No	No	Yes	No	No	No
Bubbles polydisperse	No	No	No	Yes	No	No
Loading averaged	Yes	No	No	No	No	Yes
Clustering considered	No	No	No	No	Yes	Yes
Simulation time	Very low	Low	Medium	Medium	Very high	Low
Complexity	Very low	Low	Medium	Medium	High	Low
Standard deviation of bubble diameter	Small	Small	Small	High	Small	Small
Standard deviation of cell diameter	Small	Small	High	Small	Small	Small
Influence of clustering	Negligible	Negligible	Negligible	Negligible	Important	Important
Cells have to be smaller than bubbles	Yes	Yes	Yes	Yes	No	No
Difficulty of direct coupling to CFD simulations	Low	High	High	High	Very high	Medium

Preprints (www.preprints.org) | NOT PEER-REVIEWED | Posted: 22 August 2018 doi:10.20944/preprints201808.0396.v1

Peer-reviewed version available at Processes 2018, 6, 184; doi:10.3390/pr6100184

4.2.2. Aggregation mechanisms

The aggregation kernel $\beta(d_{b,St}, d_{c,St})$ of unloaded bubbles and free cells is illustrated as a function of time on the investigated streamline in Figure 6a.

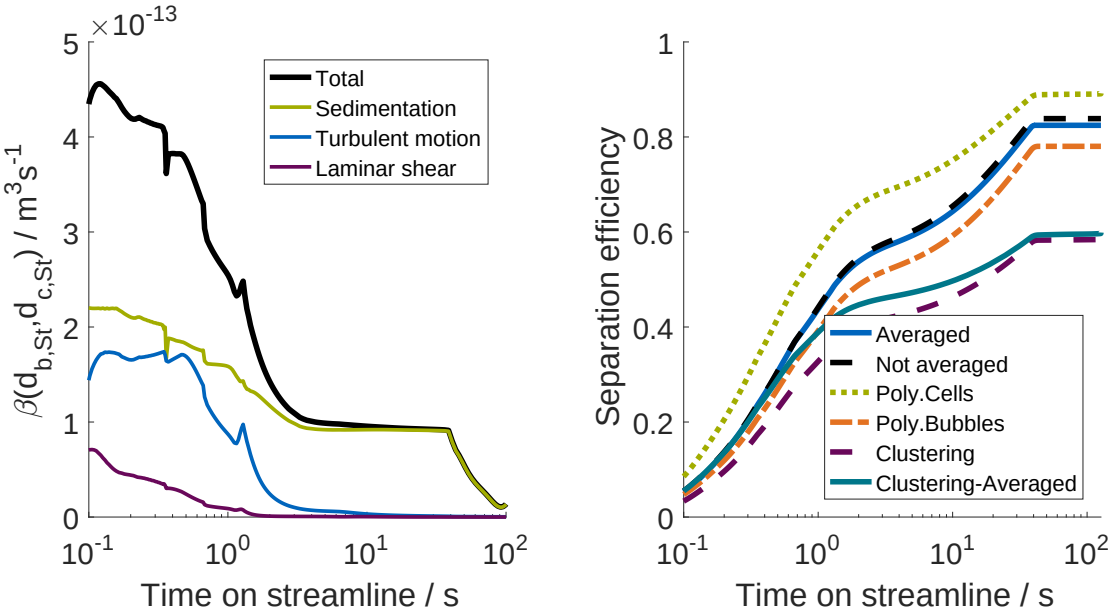

(a) Importance of aggregation mechanisms on a single streamline

(b) Separation efficiencies for different aggregation models

Figure 6. Aggregation mechanisms on a single streamline and resulting separation efficiencies for different aggregation models for this streamline

The total aggregation kernel for the streamline is high in the first 3 seconds. Then it stays nearly constant until approximately 40 seconds. Between 40 and 90 seconds, β decreases. Then, close to the outlet, β increases again. During the first 2 seconds the aggregation due to turbulent motion and laminar shear has a noticeable influence on the total aggregation kernel. Afterwards, sedimentation is the only important aggregation mechanism. The aggregation kernel depends on the hydrodynamic encounter efficiency, which depends on the gas volume fraction. Therefore, when the gas volume fraction decreases after 40 seconds, the aggregation kernel decreases as well. The last 50 seconds (not shown here), the aggregation kernel increases again, since the fluid velocity increases in the region of the outlet. However, this part is not important for the aggregation process, since in this region, the gas volume fraction is already zero, and no aggregation between bubbles and cells can occur. The results for other streamlines (data not shown) are similar.

4.2.3. Comparison of different aggregation models

In this section, the separation efficiencies of the investigated streamline are calculated for different aggregation models. The relative standard deviations of the bubble diameter and the cell diameter for the models *Poly.Cells* and *Poly.Cells* are $\sigma_{rel} = 0.25$. In Figure 6b, the separation efficiencies of the investigated streamline are illustrated. The efficiency for the model *Averaged* increases quickly in the first 3 seconds and reaches an efficiency of about 0.6. Then, the efficency levels off until at a residence time of approximately 40 seconds the efficiency reaches about 0.8. The trend of the flotation efficiency is the same for all aggregation models. The fast aggregation process during the first few seconds can be explained by the high gas volume fraction and the high aggregation kernel during this time. Then the rate of increase of the efficency declines, since the gas volume fraction and the aggregation kernel

decrease. At a residence time of 40 seconds, the gas volume fraction drops to zero and there is no aggregation any longer. The efficiencies of the models *Not Averaged* and *Averaged* are comparable. The efficiency of the model with polydisperse bubbles is smaller than the efficiency of the model *Averaged*, since most of the bubbles' volume is distributed for larger bubble sizes in the used gamma distribution for the bubbles. Large bubbles result in high Π_1 and are less efficient in floating cells. In contrast, the efficiency for the model *Poly.Cells* is higher than the efficiency for the model *Averaged*. This is caused by the fact, that most of the cell mass is distributed for larger cells. With an increasing cell diameter, the aggregation kernel increases and Π_1 decreases. Both effects lead to an increased flotation efficiency. The formation of clusters reduces the available surface area of bubbles and reduces the frequency of the attachment of cells. Therefore, the clustering models show lower separation efficiencies. The results for the other streamlines (data not shown) are similar.

5. Conclusion

Down-stream separation of microorganisms using DAF or microflotation lacks applicable rigorous modeling approaches for the heteroaggregation between microorganisms and microbubbles. Therefore, different mechanistic aggregation models were introduced in the present study. Three models were adapted from literature and three new were derived. The models allowed representing the distributed character of bubble and cell sizes as well as the formation of clusters consisting of several bubbles and cells. To determine the impact of the model assumptions, the modeling approaches were compared and classified for their range of applicability. Additionally, the different aggregation models were coupled to CFD data of a commercially available DAF system (Enviplan: AQUATECTOR®Microfloat®Rundzelle).

From model comparison it can be deduced, that turbulence and laminar shear form aggregates consisting of several bubbles, whereas differential sedimentation only forms aggregates consisting of a single bubble and multiple cells. The formation of aggregates with several bubbles decreases the available surface, at which cells can aggregate. This lowers the separation efficiency. Additionally, model comparisons show that bubble and cell size distributions can influence the separation efficiency significantly and should be considered to determine efficient plant configurations and operating conditions.

Once a suitable aggregation model has been selected from the discussed options, the flotation process can be optimized computationally for separating the microorganisms. In this study the encounter efficiency due to attractive and repulsive forces $P_{A,0}$ was assumed to be unity. In an extension to this paper, $P_{A,0}$ should be determined as described in the modeling section. This requires detailed knowledge about the process conditions or experimental data. CFD data suggest, that the classical two zone model is not accurate since fluid dynamics are highly heterogeneous in the flotation tank. Thus, the aggregation models should be combined with the proposed Lagrangian approach or directly coupled to CFD of the flotation process to determine efficient plant configurations and process conditions. Direct coupling to CFD can be easily performed with the new developed averaged approaches.

Author Contributions: S.R. provided the research idea; S.S, C.K., S.R., J.H. and H.B. conceptualized the work; S.S. wrote the initial draft of the article and performed the PBM simulations; C.K. and H.B. supervised S.S.; J.H. performed the CFD simulations; S.S, C.K., S.R., J.H. and H.B. discussed and interpreted the results and wrote the final paper.

Funding: The authors thank BASF SE for the financial support for this work.

Acknowledgments: We thank Dr. Christian Riedele and Susanne Gulden for stimulating discussions.

Conflicts of Interest: The authors declare no conflict of interest.

Appendix A. Model *Averaged* - Algebraic solution for two zone model

In this section, the analytical solution for the model *Averaged* is deduced for a plug flow.

Aggregation equation

The general equation for aggregation for the model *Averaged* is

$$\frac{\mathrm{d}c_c}{\mathrm{d}t} = -\beta(d_{c,0}, d_b) \cdot c_c \cdot c_b. \tag{A1}$$

Collision efficiency due to surface coverage

The total surface area a_b of all bubbles per unit volume can be obtained by multiplying the surface area of a single bubble with the bubble number concentration

$$a_b = \pi \cdot d_b^2 \cdot c_b. \tag{A2}$$

The total projected surface area a_c of cells bound to bubbles per unit volume is

$$a_c = \frac{\pi}{4} \cdot d_{c,0}^2 \cdot (c_{c,0} - c_c)\,, \tag{A3}$$

The collision efficiency due to surface coverage is assumed to be proportional to the fraction of the non-occupied surface area of the bubbles.

$$\begin{aligned} P_{A,S} &= \frac{a_b - a_c}{a_b} && \text{(A4)}\\ &= 1 - \frac{\frac{\pi}{4} \cdot d_{c,0}^2 \cdot (c_{c,0} - c_c)}{\pi \cdot d_b^2 \cdot c_b} && \text{(A5)}\\ &= 1 - \frac{c_{c,0} \cdot d_{c,0}^2}{4 \cdot c_{b,0} \cdot d_b^2} \cdot \left(1 - \frac{c_c}{c_{c,0}}\right). && \text{(A6)} \end{aligned}$$

Non-dimensionalization

First of all, the following non-dimensional variables are useful

$$\begin{aligned} \tilde{c}_c &= \frac{c_c}{c_{c,0}} && \text{(A7)}\\ \tilde{c}_b &= \frac{c_b}{c_{b,0}} && \text{(A8)}\\ \tilde{d}_b &= \frac{d_b}{d_{b,0}}, && \text{(A9)} \end{aligned}$$

Substituting these non-dimensional variables into the efficiency due to surface coverage yields

$$P_{A,\mathrm{surface}} = 1 - \frac{\Pi_1}{\tilde{c}_b \tilde{d}_b^2} (1 - \tilde{c}_c)\,. \tag{A10}$$

$$\begin{aligned} P_{A,\mathrm{surface}} =& 1 - \frac{c_{c,0} \cdot d_{c,0}^2}{4 \cdot d_b^2 \cdot c_b} \cdot \left(1 - \frac{c_c}{c_{c,0}}\right)\\ =& 1 - \frac{c_{c,0} \cdot d_{c,0}^2}{4 \cdot d_{b,0}^2 \cdot c_{b,0}} \cdot \frac{1 - \tilde{c}_c}{\tilde{c}_b \cdot \tilde{d}_b^2}\\ =& 1 - \frac{\Pi_1}{\tilde{c}_b \tilde{d}_b^2} (1 - \tilde{c}_c)\,, \end{aligned} \tag{A11}$$

where Π_1 is a dimensionless group. Π_1 can be expressed as:

$$\Pi_1 = \frac{1}{4} \cdot \frac{c_{c,0} \cdot d_{c,0}^2}{c_{b,0} \cdot d_{b,0}^2}. \tag{A12}$$

Using

$$\beta(d_{c,0}, d_b) = P_{A,surface} \cdot K(d_{c,0}, d_b), \tag{A13}$$

the equation,which describes the general aggregation equation, can be transformed as follows:

$$\frac{\mathrm{d}c_c}{\mathrm{d}t} = -P_{A,surface} \cdot K(d_{c,0}, d_b) \cdot c_c \cdot c_b \tag{A14}$$

$$\Leftrightarrow \frac{\mathrm{d}\tilde{c}_c}{\mathrm{d}t} = -\left(1 - \frac{\Pi_1}{\tilde{c}_b \tilde{d}_b^2}(1 - \tilde{c}_c)\right) \cdot K\left(\frac{d_{c,0}}{d_{b,0}} \cdot d_{b,0}, d_{b,0} \cdot \tilde{d}_b\right) \cdot c_{b,0} \cdot \tilde{c}_c \cdot \tilde{c}_b. \tag{A15}$$

Implementing the dimensionless time τ, the ratio of diameters of cells and bubbles Π_2 and the normalized aggregation frequency $\tilde{K}$

$$\tau = t \cdot K(d_{b,0} \cdot \Pi_2, d_{b,0}) \cdot c_{b,0} \tag{A16}$$

$$\Pi_2 = \frac{d_{c,0}}{d_{b,0}} \tag{A17}$$

$$\tilde{K} = \frac{K(d_{b,0} \cdot \Pi_2, d_{b,0} \cdot \tilde{d}_b)}{K(d_{b,0} \cdot \Pi_2, d_{b,0})} \tag{A18}$$

one can transform the general aggregation equation

$$\frac{\mathrm{d}\tilde{c}_c}{\mathrm{d}\tau} = -\left(1 - \frac{\Pi_1}{\tilde{c}_b \cdot \tilde{d}_b^2}(1 - \tilde{c}_c)\right) \cdot \tilde{K} \cdot \tilde{c}_c \cdot \tilde{c}_b. \tag{A19}$$

A dimensionless group Π_3 can be obtained - the aggregation number

$$\Pi_3 = t_{residence} \cdot K(d_{b,0} \cdot \Pi_2, d_{b,0}) \cdot c_{b,0}. \tag{A20}$$

Analytical solution

Neglecting bubble coalescence, the concentration and diameter of the bubbles stay constant. Furthermore, it is assumed that the aggregates have the diameter of a single bubble. Therefore $\tilde{c}_b(\tau) = 1$ and $\tilde{d}_b(\tau) = 1$, which leads to $\tilde{K} = 1$. The equation describing aggregation can be simplified to:

$$\frac{\mathrm{d}\tilde{c}_c}{\mathrm{d}\tau} = -(1 - \Pi_1 \cdot (1 - \tilde{c}_c)) \cdot \tilde{c}_c. \tag{A21}$$

By analytically integrating this differential equation from $\tau = 0$ to $\tau = \Pi_3$ ($t = t_{residence}$), the cell concentration at the end of the contact zone $\tilde{c}_{c,out}$ can be calculated as:

$$\tilde{c}_{c,out} = \frac{1 - \Pi_1}{\exp(\Pi_3 \cdot (1 - \Pi_1)) - \Pi_1}. \tag{A22}$$

Appendix B. Encounter efficiency due to surface coverage for clustering

To consider the reduction of the encounter efficiency due to surface coverage in the models *Clustering* and *Clustering Averaged*, some assumptions have do be made. First of all, it is assumed that

the cells of a cluster are uniformly distributed on the surface of all bubbles of the cluster. Moreover, the clusters are packed densely. An attachment between two clusters can only occur if a cell of the exposable surface area of a cluster collides with a bubble of the exposable surface area of the other cluster or vice versa. Since bubble coalescence and aggregation is negligible [12], the aggregation between bubbles is assumed to be impossible. Furthermore, the coagulation of cells is neglected. Otherwise flocks would be formed and microflotation would not be necessary. With the assumption that clusters are densely packed, the volume of a cluster consisting of i bubbles and j cells can be calculated as the sum of the volume of the consisting bubbles and cells

$$V_{i,j} = i \cdot V_b + j \cdot V_c = \frac{1}{6} \cdot \pi \left(i \cdot d_b^3 + j \cdot d_c^3 \right). \tag{A23}$$

Additionally, the cluster volume can be described as

$$V_{i,j} = \frac{1}{6} \cdot \pi \cdot d_{i,j}^3, \tag{A24}$$

where $d_{i,j}$ is the cluster's equivalent diameter. Setting Equation (A23) equal to Equation (A24), $d_{i,j}$ can be expressed as

$$d_{i,j} = \left(i \cdot d_b^3 + j \cdot d_c^3 \right)^{\frac{1}{3}}. \tag{A25}$$

The exposed surface area of a cluster with i bubbles and j cells $A_{exposed}(i,j)$ is expressed as

$$A_{exposed}(i,j) = \pi \cdot d_{i,j}^2 = \pi \cdot \left(i \cdot d_b^3 + j \cdot d_c^3 \right)^{\frac{2}{3}}. \tag{A26}$$

The sum of the surface area of all bubbles of a cluster with i bubbles $A_{b,surface}(i,j)$ is calculated as

$$A_{b,surface}(i,j) = i \cdot \pi \cdot d_b^2. \tag{A27}$$

The sum of the projected surface area of j cells of a cluster $A_{c,proj}(i,j)$ is expressed as

$$A_{c,proj}(i,j) = j \cdot \frac{\pi}{4} \cdot d_c^2. \tag{A28}$$

Assuming that the cells of a cluster are uniformly distributed on the surface of all bubbles of the cluster, the ratio of the exposed cluster surface which is occupied by cells $R_p(i,j)$ is calculated as

$$R_p(i,j) = \frac{A_{c,proj}(i,j)}{A_{b,surface}(i,j)} = \frac{j \cdot d_c^2}{i \cdot 4 \cdot d_b^2}. \tag{A29}$$

Knowing $R_p(i,j)$ the ratio of the exposable cluster surface which is occupied by bubbles $R_b(i,j)$ can be expressed by

$$R_b(i,j) = 1 - R_p(i,j). \tag{A30}$$

References

1. Christenson, L.; Sims, R. Production and harvesting of microalgae for wastewater treatment, biofuels, and bioproducts. *Biotechnology advances* **2011**, *29*, 686–702.
2. Sarris, D.; Papanikolaou, S. Biotechnological production of ethanol: Biochemistry, processes and technologies. *Engineering in Life Sciences* **2016**, *16*, 307–329.
3. Chisti, Y. Biodiesel from microalgae. *Biotechnology advances* **2007**, *25*, 294–306.
4. Larkum, A.W.; Ross, I.L.; Kruse, O.; Hankamer, B. Selection, breeding and engineering of microalgae for bioenergy and biofuel production. *Trends in biotechnology* **2012**, *30*, 198–205.
5. Grima, E.M.; Belarbi, E.H.; Fernández, F.A.; Medina, A.R.; Chisti, Y. Recovery of microalgal biomass and metabolites: process options and economics. *Biotechnology advances* **2003**, *20*, 491–515.

6. Barros, A.I.; Gonçalves, A.L.; Simões, M.; Pires, J.C. Harvesting techniques applied to microalgae: A review. *Renewable and Sustainable Energy Reviews* **2015**, *41*, 1489–1500.
7. Soetaert, W.; Vandamme, E.J. *Industrial biotechnology: sustainable growth and economic success*; John Wiley & Sons, 2010.
8. Ndikubwimana, T.; Chang, J.; Xiao, Z.; Shao, W.; Zeng, X.; Ng, I.S.; Lu, Y. Flotation: A promising microalgae harvesting and dewatering technology for biofuels production. *Biotechnology journal* **2016**, *11*, 315–326.
9. Hanotu, J.; Bandulasena, H.; Zimmerman, W.B. Microflotation performance for algal separation. *Biotechnology and bioengineering* **2012**, *109*, 1663–1673.
10. Hanotu, J.; Karunakaran, E.; Bandulasena, H.; Biggs, C.; Zimmerman, W.B. Harvesting and dewatering yeast by microflotation. *Biochemical Engineering Journal* **2014**, *82*, 174–182.
11. Shawwa, A.R.; Smith, D.W. Dissolved air flotation model for drinking water treatment. *Canadian Journal of Civil Engineering* **2000**, *27*, 373–382.
12. Edzwald, J.K. Dissolved air flotation and me. *Water Research* **2010**, *44*, 2077–2106.
13. Fukushi, K.; Tambo, N.; Matsui, Y. A Kinetic-Model for Dissolved Air Flotation in Water and Waster-Water Treatment. *Water Science and Technology* **1995**, *31*, 37–47. International Specialised Conference on Flotation Processes in Water and Sludge Treatment, Orlando.
14. Leppinen, D.; Dalziel, S. Bubble size distribution in dissolved air flotation tanks. *Journal of Water Supply Research and Technology - AQUA* **2004**, *53*, 531–543.
15. Liers, S.; Baeyens, J.; Mochtar, I. Modeling dissolved air flotation. *Water Environment Research* **1996**, *68*, 1061–1075.
16. Kwak, D.H.; Yoo, S.J.; Lee, E.J.; Lee, J.W. Evaluation on simultaneous removal of particles and off-flavors using population balance for application of powdered activated carbon in dissolved air flotation process. *Water Science and Technology* **2010**, *61*, 323–330.
17. Jung, H.; Lee, J.; Choi, D.; Kim, S.; Kwak, D. Flotation efficiency of activated sludge flocs using population balance model in dissolved air flotation. *Korean Journal of Chemical Engineering* **2006**, *23*, 271–278.
18. Laamanen, C.A.; Ross, G.M.; Scott, J.A. Flotation harvesting of microalgae. *Renewable and Sustainable Energy Reviews* **2016**, *58*, 75–86.
19. Zhang, X.; Wang, L.; Sommerfeld, M.; Hu, Q. Harvesting microalgal biomass using magnesium coagulation-dissolved air flotation. *Biomass and Bioenergy* **2016**, *93*, 43–49.
20. Zhang, X.; Hewson, J.C.; Amendola, P.; Reynoso, M.; Sommerfeld, M.; Chen, Y.; Hu, Q. Critical evaluation and modeling of algal harvesting using dissolved air flotation. *Biotechnology and Bioengineering* **2014**, *111*, 2477–2485.
21. Leppinen, D.; Dalziel, S.; Linden, P. Modelling the global efficiency of dissolved air flotation. *Water Science and Technology* **2001**, *43*, 159–166. 4th International Conference on Dissolved Air Flotation in Water and Waste Water Treatment, Helsinki, Finland.
22. Kwak, D.H.; Jung, H.J.; Kwon, S.B.; Lee, E.J.; Won, C.H.; Lee, J.W.; Yoo, S.J. Rise velocity verification of bubble-floc agglomerates using population balance in the DAF process. *Journal of Water Supply Research and Technology - AQUA* **2009**, *58*, 85–94.
23. Matsui, Y.; Fukushi, K.; Tambo, N. Modeling, simulation and operational parameters of dissolved air flotation. *Journal of Water Services Research and Technology - AQUA* **1998**, *47*, 9–20.
24. Lakghomi, B.; Lawryshyn, Y.; Hofmann, R. A model of particle removal in a dissolved air flotation tank: Importance of stratified flow and bubble size. *Water Research* **2015**, *68*, 262–272.
25. Kostoglou, M.; Karapantsios, T.D.; Matis, K.A. CFD model for the design of large scale flotation tanks for water and wastewater treatment. *Industrial & Engineering Chemistry Research* **2007**, *46*, 6590–6599.
26. Edzwald, J.K. Principles and applications of dissolved air flotation. *Water Science and Technology* **1995**, *31*, 1–23. International Specialised Conference on Flotation Processes in Water and Sludge Treatment, Orlando, FL, Apr 26-28, 1994.
27. Saffman, P.; Turner, J. On the collision of drops in turbulent clouds. *Journal of Fluid Mechanics* **1956**, *1*, 16–30.
28. Meyer, C.; Deglon, D. Particle collision modeling - A review. *Minerals Engineering* **2011**, *24*, 719 – 730.
29. Pedocchi, F.; Piedra-Cueva, I. Camp and Stein's Velocity Gradient Formalization. *Journal of Environmental Engineering* **2005**, *131*, 1369–1376.
30. von Smoluchowski, M. Versuch einer mathematischen Theorie der Koagulationskinetik kolloider Lösungen. *Zeitschrift für physikalische Chemie* **1917**, *92*, 129–168.

31. Nguyen, A.; Ralston, J.; Schulze, H. On modelling of bubble-particle attachment probability in flotation. *International Journal of Mineral Processing* **1998**, *53*, 225–249.
32. Nguyen, A. Hydrodynamics of liquid flows around air bubbles in flotation: a review. *International Journal of Mineral Processing* **1999**, *56*, 165–205.
33. Sasic, S.; Sibaki, E.K.; Strom, H. Direct numerical simulation of a hydrodynamic interaction between settling particles and rising microbubbles. *European Journal of Mechanics B - Fluids* **2014**, *43*, 65–75. doi:10.1016/j.euromechflu.2013.07.003.
34. Dai, Z.; Fornasiero, D.; Ralston, J. Particle-bubble collision models - a review. *Advances in Colloid and Interface Science* **2000**, *85*, 231 – 256.
35. Rollié, S.; Briesen, H.; Sundmacher, K. Discrete bivariate population balance modelling of heteroaggregation processes. *Journal of Colloid and Interface Science* **2009**, *336*, 551–564.
36. Ren, Z.; Harshe, Y.M.; Lattuada, M. Influence of the Potential Well on the Breakage Rate of Colloidal Aggregates in Simple Shear and Uniaxial Extensional Flows. *Langmuir* **2015**, *31*, 5712–5721.
37. Sun, W.; Zeng, Q.; Yu, A. Calculation of Noncontact Forces between Silica Nanospheres. *Langmuir* **2013**, *29*, 2175–2184.
38. Rudolph, M.; Peuker, U.A. Hydrophobicity of Minerals Determined by Atomic Force Microscopy - A Tool for Flotation Research. *Chemie Ingenieur Technik* **2014**, *86*, 865–873.
39. Ta, C.; Beckley, J.; Eades, A. A multiphase CFD model of DAF process. *Water Science and Technology* **2001**, *43*, 153–157. 4th International Conference on Dissolved Air Flotation in Water and Waste Water Treatment.
40. Tomiyama, A.; Takamasa, T. *Ansys 16.2.3; Interphase Exchange Coefficients: Tomiyama et al. Model (17.5.6.1.5.)*.
41. Kumar, J.; Peglow, M.; Warnecke, G.; Heinrich, S.; Morl, L. Improved accuracy and convergence of discretized population balance for aggregation: The cell average technique. *Chemical Engineering Science* **2006**, *61*, 3327–3342.
42. Iyer-Biswas, S.; Crooks, G.E.; Scherer, N.F.; Dinner, A.R. Universality in stochastic exponential growth. *Physical review letters* **2014**, *113*.